AIP | The Journal of Chemical Physics

Intersystem crossing rates of S1 state keto-amino cytosine at low excess energy

Simon Lobsiger, Mihajlo Etinski, Susan Blaser, Hans-Martin Frey, Christel Marian, and Samuel Leutwyler

Citation: The Journal of Chemical Physics **143**, 234301 (2015); doi: 10.1063/1.4937375
View online: http://dx.doi.org/10.1063/1.4937375
View Table of Contents: http://scitation.aip.org/content/aip/journal/jcp/143/23?ver=pdfcov
Published by the AIP Publishing

Intersystem crossing rates of S_1 state keto-amino cytosine at low excess energy

Simon Lobsiger,[1] Mihajlo Etinski,[2] Susan Blaser,[1] Hans-Martin Frey,[1] Christel Marian,[3] and Samuel Leutwyler[1,a)]

[1]*Departement für Chemie und Biochemie, Universität Bern, Freiestrasse 3, CH-3012 Bern, Switzerland*
[2]*Fakultet za Fizičku Hemiju, Univerzitet u Beogradu, Studentski Trg 12-16, SRB-11000 Beograd, Serbia*
[3]*Institut für Theoretische Chemie und Computerchemie, Heinrich-Heine Universität, Universitätsstrasse 1, D-40225 Düsseldorf, Germany*

(Received 24 August 2015; accepted 24 November 2015; published online 15 December 2015)

The amino-keto tautomer of supersonic jet-cooled cytosine undergoes intersystem crossing (ISC) from the $v = 0$ and low-lying vibronic levels of its $S_1(^1\pi\pi^*)$ state. We investigate these ISC rates experimentally and theoretically as a function of S_1 state vibrational excess energy E_{exc}. The S_1 vibronic levels are pumped with a ~5 ns UV laser, the S_1 and triplet state ion signals are separated by prompt or delayed ionization with a second UV laser pulse. After correcting the raw ISC yields for the relative S_1 and T_1 ionization cross sections, we obtain energy dependent ISC quantum yields $Q_{ISC}^{corr} = 1\%–5\%$. These are combined with previously measured vibronic state-specific decay rates, giving ISC rates $k_{ISC} = 0.4–1.5 \cdot 10^9$ s^{-1}, the corresponding $S_1 \rightsquigarrow S_0$ internal conversion (IC) rates are 30–100 times larger. Theoretical ISC rates are computed using SCS-CC2 methods, which predict rapid ISC from the $S_1; v = 0$ state with $k_{ISC} = 3 \cdot 10^9$ s^{-1} to the $T_1(^3\pi\pi^*)$ triplet state. The surprisingly high rate of this El Sayed-forbidden transition is caused by a substantial admixture of $^1n_O\pi^*$ character into the $S_1(^1\pi\pi^*)$ wave function at its non-planar minimum geometry. The combination of experiment and theory implies that (1) below $E_{exc} = 550$ cm^{-1} in the S_1 state, $S_1 \rightsquigarrow S_0$ internal conversion dominates the nonradiative decay with $k_{IC} \geq 2 \cdot 10^{10}$ s^{-1}, (2) the calculated $S_1 \rightsquigarrow T_1$ ($^1\pi\pi^* \rightsquigarrow ^3\pi\pi^*$) ISC rate is in good agreement with experiment, (3) being El-Sayed forbidden, the $S_1 \rightsquigarrow T_1$ ISC is moderately fast ($k_{ISC} = 3 \cdot 10^9$ s^{-1}), and not ultrafast, as claimed by other calculations, and (4) at $E_{exc} \sim 550$ cm^{-1} the IC rate increases by ~50 times, probably by accessing the lowest conical intersection (the C5-twist CI) and thereby effectively switching off the ISC decay channels. © *2015 AIP Publishing LLC.* [http://dx.doi.org/10.1063/1.4937375]

I. INTRODUCTION

The canonical pyrimidine nucleobase cytosine (Cyt) pairs with guanine within double-stranded DNA, and its derivatives play an important role in epigenetics and medicine. In aqueous solution, cytosine is highly stable against UV irradiation. The fact that cytosine has survived photolysis by the intense UV solar radiation on early Earth has been taken to imply photochemical selection of the molecular building blocks of life.[1–5] In this context it is important to investigate the radiationless relaxation rates of the biologically relevant keto-amino cytosine tautomer. The $^1\pi\pi^*$ state lifetimes of cytosine derivatives in aqueous buffer solutions have been measured by femtosecond (fs) transient absorption and fs fluorescence upconversion methods,[6–8] to be $\tau = 1.0$ ps for cytosine,[8] $\tau = 0.7–1.0$ ps for the RNA nucleoside cytidine (Cyd),[6–8] and $\tau = 0.8–1.2$ ps for the RNA nucleotide CMP.[6–8] These values are in agreement with the fluorescence quantum yields of cytosine derivatives, which are $\leq 10^{-4}$.[9] Methylation of cytosine and cytidine at the 5-position increases the lifetimes by about seven times, $\tau = 7.2$ ps for both 5-methylcytosine and 5-methylcytidine.[8] In aqueous solution, the intersystem crossing quantum yield for triplet formation from the lowest $^1\pi\pi^*$ state of cytosine (and its derivatives) is below a few percent,[10,11] indicating that nonradiative decay by internal conversion (IC) is the dominant nonradiative relaxation pathway of the $^1\pi\pi^*$ state of cytosine and its derivatives.[5]

In the gas phase, the situation is different: De Vries and co-workers have measured the resonant two-photon ionization (R2PI) spectra of supersonically jet-cooled cytosine, 5-methylcytosine and 1-methylcytosine and assigned the R2PI spectrum of cytosine near 32 000 cm^{-1} to the $S_0 \rightarrow S_1$ ($^1\pi\pi^*$) transition of the keto-amino N1H tautomer.[12–14] They noted that excitation of the cytosine $^1\pi\pi^*$ state leads to a long-lived state with $\tau = 290$ ns, which they tentatively assigned to a triplet state.[12–14] Recent R2PI spectroscopic investigations of the lowest $^1\pi\pi^*$ transition of keto-amino cytosine have confirmed that the long-lived dark state of cytosine is indeed efficiently formed and that the energy of the dark state, determined via its photoionization threshold using pump-delayed probe photoionization, agrees almost perfectly with the theoretically predicted T_1 state energy.[15,16] However, there is so far no direct experimental evidence (such as polarization or magnetic field dependence) of the triplet nature of the long-lived state.

a)E-mail: leutwyler@dcb.unibe.ch

Numerous theoretical studies of the excited-state dynamics and decay mechanisms of Cyt have been reported, most of which have focused on the keto-amino tautomer **1** (see Figure 1) because of its biological importance.[1,17–33] The minimum of the lowest $^1\pi\pi^*$ state of **1** has been shown to be connected to three different conical intersections (CIs) with the S_0 surface; all three involve some degree of out-of-plane deformation of the pyrimidine ring. Tomić *et al.* calculated the vertical and adiabatic absorption energies of the keto, enol, and keto-imino tautomers of cytosine.[19] They determined density functional/multi-reference configuration interaction (DFT/MRCI) energies along the time-dependent density functional (TDDFT) reaction path that connects the excited-state $^1\pi\pi^*$ minimum and this conical intersection and found that the $^1\pi\pi^*$ minimum is separated by a 1600 cm^{-1} (0.2 eV) barrier from the CI.[19] Two recent excited-state dynamics studies including non-adiabatic as well as spin–orbit coupling claimed the decay of the S_1 population via ISC to the T_2 state to be ultrafast.[32,33] At least for vibrationally cold S_1 cytosine, this result contradicts the recent experimental findings by Lobsiger *et al.*[15,16] For the pyrimidine bases uracil and thymine, Etinski *et al.* carried out combined coupled-cluster and DFT/MRCI calculations to determine ISC rate constants.[34] They predicted ISC to play an important role in the electronic relaxation from the initially excited $^1\pi\pi^*$ state in the gas phase. This was later confirmed experimentally.[35] The predictive power of that theoretical study motivated us to reinvestigate the excited-state processes in the biologically relevant keto-amino cytosine by means of approximate coupled-cluster methods, with a focus on ISC.

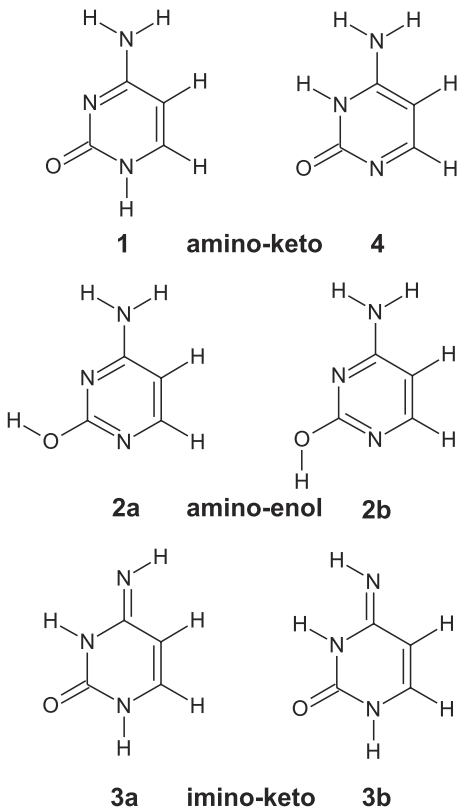

FIG. 1. The six most stable tautomers of gas-phase cytosine.

Femtosecond (fs) pump-probe time-resolved ionization and photoelectron spectroscopic experiments have been performed on thermally vaporized and jet-cooled cytosine.[36–40] The early measurements[36] found sub-picosecond to picosecond lifetimes with mono- or biexponential decay profiles. Ullrich *et al.* noted that both keto and enol tautomers of cytosine contribute to the signals observed.[37] However, these measurements employed excitation at UV wavelengths (250-267 nm), at which several gas-phase tautomers can be excited. Kosma *et al.* attempted to distinguish the decay of the keto-amino tautomer **1** from those of the enol-amino (**2a, 2b**) and keto-imino (**3a, 3b**) tautomers (see Figure 1) by exciting at 280-290 nm, where only **1** absorbs UV light.[39] At 280 nm they fitted lifetimes of τ = 1.2 ps and at 290 nm of τ = 1.1 ps. Cheng and co-workers performed fs pump-probe measurements up to 300 nm and observed τ = 1.5 ps.[40] However, even at 300 nm the keto-amino tautomer **1** is excited far above its lowest conical intersection (the C5-C6 "twist" CI) in the $S_1(^1\pi\pi^*)$ state.

Recently, Lobsiger *et al.* have determined the lifetimes of the lowest $S_1(^1\pi\pi^*)$ state vibronic levels with excess energies E_{exc} = 0–550 cm^{-1} by measuring the Lorentzian broadening of the rovibronic band contours.[16] The lifetime at the 0_0^0 band is $\tau \geq 44 \pm 5$ ps and remains in the 30–45 ps range up to the $2\nu_3'$ level at +205 cm^{-1}. This decay rate is ~30-40 times slower than the nonradiative rates measured by fs time-resolved pump-ionization measurements,[36–40] signaling much slower nonradiative dynamics for the vibrational levels that are localized near the $S_1(^1\pi\pi^*)$ minimum. The levels in the range 308–447 cm^{-1} have lifetimes $\tau \sim 25$ ps, the 6*a* level lifetime at E_{exc} = 530 cm^{-1} was estimated to be 3–6 ps.[16] No vibronic bands are observed above 530 cm^{-1}, implying an upper lifetime limit of $\tau < 2$ ps for these levels. Trachsel *et al.* have performed analogous lifetime measurements for 5-methylcytosine.[41]

II. COMPUTATIONAL METHODS AND RESULTS

A. Computational methods

We employed the spin-component scaled coupled-cluster method with approximate treatment of doubles (SCS-CC2) for electronic structure calculations. Spin-component scaling assumes different scaling of energy contributions of the same- and opposite-spin components. This scaling enhances the accuracy of 0-0 transition energies both for $\pi\pi^*$ and $n\pi^*$ states.[42] In a recent benchmark study, it was shown that the standard deviation of 0-0 transition energies for a set of organic molecules is 0.06 eV.[43] For the calculations of SCS-CC2 energies we used the standard scaling factors 1/3 for the same-spin and 6/5 for the opposite-spin components.

The calculations were performed with the TURBOMOLE program.[44] We used the resolution-of-identity (RI)[45] CC2 implementation in TURBOMOLE[46] for the ground state[47] and the corresponding linear response theory version for excited-state optimizations[48] and vertical excitation energies and the calculation of properties.[49] In all calculations, only valence electrons were correlated. Throughout, Dunning's[50,51] augmented correlation-consistent basis set (aug-cc-pVTZ)

was employed. Auxiliary basis sets for the RI approximation of the two-electron integrals were taken from the TURBOMOLE library.[52] The SNF[53] program was used for numerical calculations of vibrational frequencies in harmonic approximation.

In previous work on thymine and uracil,[34] we had combined potential energy surfaces from CC2 calculations and spin–orbit matrix elements (SOMEs) obtained from DFT/MRCI wave functions to determine ISC rate constants. This procedure seemed inappropriate here because the SCS-CC2 and the DFT/MRCI calculations gave substantially different electronic structures of the excited states. In particular, the relative weights of $\pi\pi^*$ and $n\pi^*$ configurations, which are crucial for the size of the SOMEs, were found to differ largely. For this reason, we decided to use the amplitudes of the SCS-CC2 wave functions to determine the SOMEs.

The fact that linear response calculations yield non-zero amplitudes only for those configurations that are singly excited with respect to the electronic ground (S_0) state facilitates the evaluation of SOMEs. Thus, for each configuration only a single spin-adapted configuration state function (CSF) contributes. For triplets, the two open shells are chosen to be occupied by electrons with α spins, i.e., $(\alpha(1)\alpha(2))$, whereas in the singlet case a linear combination of two determinants is necessary to represent the CSF, i.e., $(\alpha(1)\beta(2) - \beta(1)\alpha(2))/\sqrt{2}$. Using an effective one-electron spin–orbit Hamiltonian, matrix elements $\langle {}^3\Psi_a^r|\hat{\mathcal{H}}_{\mathrm{SO}}|{}^1\Psi_b^s\rangle$ are only different from zero if $a = b$ or $r = s$. Due to the symmetry properties of the spin–orbit Hamiltonian, matrix elements vanish if $a = b$ and $r = s$. Furthermore, the antisymmetry of the spatial part of the spin–orbit integrals, i.e., $\langle a|\hat{\ell}|b\rangle = -\langle b|\hat{\ell}|a\rangle$, and a prefactor of $-1/\sqrt{2}$ from the spin part have to be taken into account in the evaluation of the SOMEs.[54] Spin–orbit integrals of the underlying Hartree-Fock molecular orbitals were evaluated using the SPOCK program[55] employing a one-center mean-field approximation to the Breit-Pauli Hamiltonian.[56,57]

With the electronic coupling matrix elements, vibrational frequencies and wave functions at hand, intersystem crossing (ISC) rates were calculated using the VIBES program.[58–61] The calculation of rates makes use of the Fermi golden-rule and harmonic multimode approximation including Dushinsky rotations. Theoretical details of the method are provided elsewhere.[59–61] In all ISC rate calculations a Gaussian damping function of width 1.0 cm^{-1} was employed.

B. Theoretical results

As stated above, we used SCS-CC2 for computing the potential energy surfaces of the ground and excited states. The reason for this choice of method was the optimized geometry of the first excited singlet state of keto-amino cytosine. SCS-CC2 was the only method that resulted in a non-planar equilibrium structure of the S_1 state, in agreement with the UV spectroscopic results.[15,16] Regular CC2 as well as TDDFT employing the B3LYP functional yielded an $n_O\pi^*$ electronic structure for the S_1 state with planar minimum geometry. For a comparison of the geometric parameters obtained at these levels of theory, see Figures S1 and S2 of the supplementary material.[62] In the following, only the SCS-CC2 results will be discussed.

The optimized geometries of all states are presented in Figure 2. Adiabatic excitation energies and 0-0 transition energies of the $S_1(\pi\pi^*)$, $T_1(\pi\pi^*)$, and $T_2(n_O\pi^*)$ states are

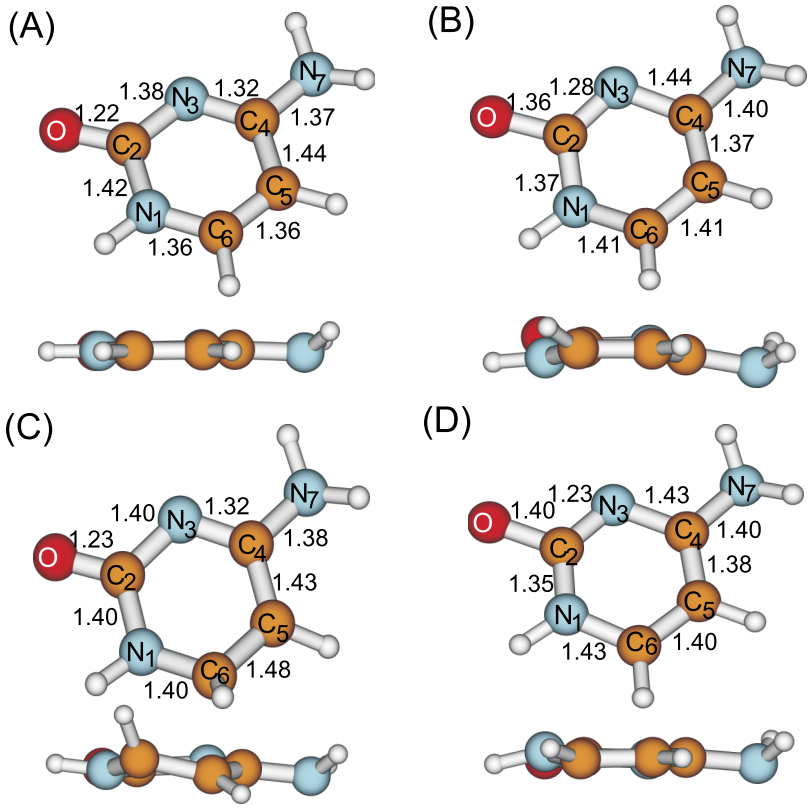

FIG. 2. The optimized geometries of keto-amino cytosine **1** at the SCS-CC2/aug-cc-pVTZ level: (a) S_0 state, (b) S_1 state, (c) T_1 state, (d) T_2 state. Bond lengths in Å.

TABLE I. Calculated and experimental adiabatic and 0-0 energies of the S_1, T_1, and T_2 electronic states of cytosine (Cyt), 5-methylcytosine (5MCyt), and 5-fluorocytosine (5FCyt).

	S_1					T_1					T_2			
Mol.	E_{adiab}	E_{0-0}	Expt.	Orbital excitation[a]	%	E_{adiab}	E_{0-0}	Expt.	Orbital exc.[a]	%	E_{adiab}	E_{0-0}	Orbital exc.[a]	%
Cyt	4.03	3.87	3.95[b]	$\pi_H \rightarrow \pi^*_L$:	29.6	3.42	3.30	3.26-3.37[c]	$\pi_H \rightarrow \pi^*_L$:	72.0	4.06	3.95	$n_{O,H} \rightarrow \pi^*_L$:	79.4
				$\pi_H \rightarrow \pi^*_{L+1}$:	21.3									
				$n_{O,H-1} \rightarrow \pi^*_L$:	16.7									
				$n_{O,H-1} \rightarrow \pi^*_{L+1}$:	12.3									
5MCyt	3.98	3.81	3.88[d]	$\pi_H \rightarrow \pi^*_{L+1}$:	39.9	3.28	3.16		$\pi_H \rightarrow \pi^*_L$:	46.8	4.27	4.17	$\pi_{H-1} \rightarrow \pi^*_L$:	49.0
				$\pi_H \rightarrow \pi^*_L$:	19.3				$\pi_H \rightarrow \pi^*_{L+1}$:	29.0				
				$n_{O,H-1} \rightarrow \pi^*_{L+1}$:	10.0									
5FCyt	3.85	3.70	3.80[e]	$\pi_H \rightarrow \pi^*_L$	62.6	3.08	2.99		$\pi_H \rightarrow \pi^*_{L+1}$:	54.7	3.91	3.81	$n_{O,H-1} \rightarrow \pi^*_{L+1}$:	78.6
				$n_{O,H-1} \rightarrow \pi^*_L$:	21.7				$\pi_H \rightarrow \pi^*_L$:	31.0			$n_{O,H-1} \rightarrow \pi^*_L$:	10.8

[a]H: HOMO, L: LUMO.
[b]Reference 16.
[c]Reference 15.
[d]Reference 41.
[e]Reference 72.

collected in Table I together with the experimental results. A comparison of vertical excitations using different quantum chemical methods is given in Table S1 of the supplementary material.[62] In the S_0 state the minimum nuclear arrangement is nearly planar, only the two hydrogen atoms connected to the N_7 atom are displaced out of ring plane. Comparing the geometry parameters to those obtained at MP2/DZP level[63] we find that our bond lengths are shorter by 0.01-0.02 Å. The adiabatic excitation energies S_1, T_1, and T_2 and the experimental adiabatic ionization energy[15] are schematically shown in Figure 3. A comparison of the calculated adiabatic excitation energies with results of previous theoretical work is given in table S2 of the supplementary material.[62]

The first excited singlet state in the adiabatic spectrum is $\pi\pi^*$, however, due to the nonplanarity of the S_1 minimum geometry the wave function contains ≈30% of $n_O\pi^*$ character. The dihedral angles $C_2N_3C_4C_5$, $C_2N_3C_4N_7$, and $C_5C_6N_1C_2$ are −17.3°, 165.0°, and −19.8°, respectively. The largest bond length changes with respect to the S_0 ground state occur for the C_2–O (+0.14 Å), C_2–N_3 (–0.10 Å), and N_3–C_4 (+0.12 Å) bonds.

Table II gives the calculated rotational constants of the S_0 and S_1 states and the $x/y/z$ ratios of the $S_0 \rightarrow S_1$ transition dipole moment components in the molecule-fixed inertial-axis frame ($a/b/c$), computed at the SCS-CC2 level. The values are in excellent agreement with experiment,[16] thus supporting our choice of method. In that experiment, the rotational contours of the 0^0_0 band and nine vibronic bands as well as the orientation of the transition dipole moment vector were found to be >95% in-plane (a/b-oriented) thereby proving that the S_1 is dominantly a $\pi\pi^*$ state.

In contrast, complete active space self-consistent field (CASSCF) yields a $n_O\pi^*$ electronic structure for the S_1 state with planar minimum nuclear arrangement.[30,64] The previously reported MS-CASPT2 optimized $^1\pi\pi^*$ geometry[63] is the S_1 global minimum as in the SCS-CC2 case. However, the MS-CASPT2 geometry is planar and its C_2–O bond (1.28 Å) is shorter than in the SCS-CC2 case.

The SCS-CC2 adiabatic $^1\pi\pi^*$ state energy (4.04 eV) can be compared to other theoretical results: It is close to the MS-CASPT2 value of 3.98 eV[63] and lower than the MRCI[65] and DFT/MRCI[19] values of 4.31 and 4.18 eV, respectively. CC2 yields an adiabatic energy of 3.78 eV for the $^1\pi\pi^*$ state while TDDFT/B3-LYP gives 3.94 eV. Note, however, that the $^1\pi\pi^*$ state corresponds to the S_2 state in both the latter cases. The SCS-CC2 zero-point energy corrected adiabatic energy is 3.87 eV, which is close to the experimental value of 3.947 eV.[15] Our attempts to optimize the singlet $n\pi^*$ state failed at the SCS-CC2 level of theory due to its close proximity with the $\pi\pi^*$ state.

The T_1 state in the adiabatic spectrum exhibits mainly $\pi\pi^*$ character. The most elongated bonds are C_6–C_5 and N_1–C_6. The ring is not planar, the $C_5C_6N_1C_2$ dihedral angle being 21.9°. Furthermore, the hydrogen atoms bound to C_6 and C_5 are twisted strongly out of plane with a HC_6C_5H dihedral angle of about 67°. The $^3\pi\pi^*$ adiabatic and zero-energy corrected energies are 3.42 and 3.30 eV, respectively. The experimentally determined T_1 energy lies in the range 3.26-3.37 eV,[15] and nicely agrees with the SCS-CC2 T_1 energy.

The second triplet state in the adiabatic spectrum is an $n_O\pi^*$ state. Its geometry is also not planar, but the out-of-plane distortions are significantly smaller than in the S_1 and T_1 states. The largest displacement with respect to the S_0 geometry is for the C–O bond length which is elongated to 1.40 Å in the T_2 state. Its adiabatic energy amounts to 4.06 eV. The zero-point energy corrected adiabatic energy is 3.95 eV. To our knowledge, experimental results are not available for this state.

With regard to ISC, we are mainly interested in the decay rate from the vibrationless v'= 0 level of the S_1 state (initial state). At the SCS-CC2 level, only the S_0 and T_1 states are located energetically below this state (Table I). According to our calculations, the lowest vibronic level of the T_2 state is only 0.08 eV (645 cm^{-1}) higher than the lowest vibronic level of the initial state. For this reason, we considered the ISC via the T_2 state as an additional possible decay channel of the S_1 population.

A detailed overview over SCS-CC2 wave function amplitudes and spin-orbit integrals over molecular orbitals is presented in Fig. S3 and Tables S3–S6 of the supplementary

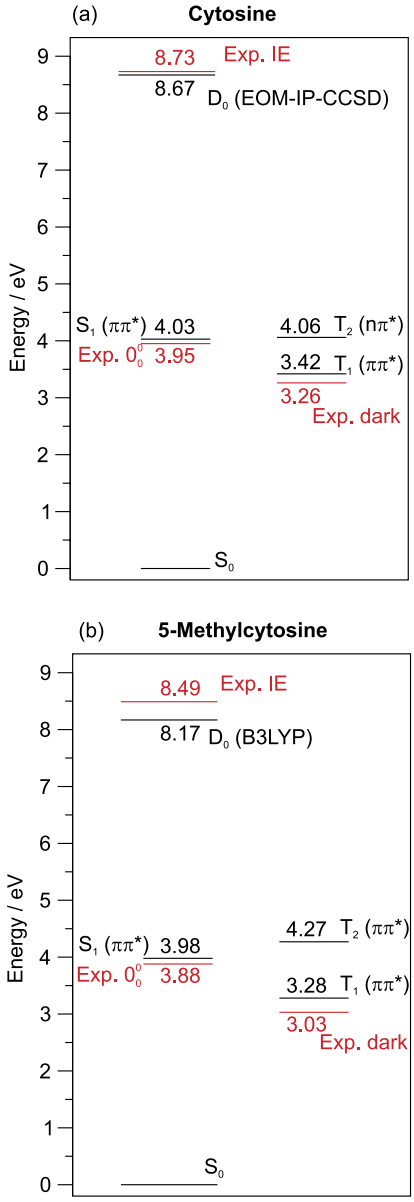

FIG. 3. Experimental (red) and SCS-CC2/aug-cc-pVTZ calculated adiabatic energies (in black) of the low-lying singlet and triplet states of the keto-amino forms of (a) cytosine and (b) 5-methylcytosine. The EOM-IP-CCSD calculated adiabatic ionization energy in (a) is taken from Ref. 75.

material.[62] The Cartesian components of the $S_1 - T_1$ SOME determined from these data at the S_1 minimum geometry amount to $12.93i$ (x), $6.56i$ (y), and $1.17i$ cm^{-1} (z), respectively. The large coupling matrix elements in x and y directions actually reflect the substantial $n_O\pi^*$ contributions to the S_1 state. Employing these values in the Condon approximation, we obtain a rate constant of $3 \cdot 10^9\ \mathrm{s}^{-1}$ for the $S_1, v = 0 \rightsquigarrow T_1$ ISC. Earlier theoretical investigations of ISC between El-Sayed forbidden transitions such as $^1\pi\pi^* \rightsquigarrow {}^3\pi\pi^*$ suggest that the Condon approximation might not be sufficient and that vibronic spin–orbit coupling might play an essential role in such cases.[58,60] We tested the influence of these higher-order coupling terms on the $S_1 \rightsquigarrow T_1$ ISC rate and found virtually no effect. The reason is probably the already quite substantial $n_O\pi^*$ contribution to the S_1 wave function.

Due to the dominant $n_O\pi^*$ character of the T_2 state, the $S_1 - T_2$ spin–orbit interaction is stronger than the $S_1 \leftrightarrow T_1$ coupling. We obtain $34.61i$ (x), $18.15i$ (y), and $2.95i$ cm^{-1} (z), respectively, for the Cartesian components of the spin–orbit Hamiltonian. Since the $S_1 \rightsquigarrow T_2$ transition is an activated process according to our SCS-CC2 calculations, we computed the ISC rate at elevated temperatures, thus populating higher vibrational levels of the S_1 state. At 300 K, the $S_1 \rightsquigarrow T_2$ ISC rate is found to be $2.3 \times 10^{10}\ \mathrm{s}^{-1}$. The small energy difference between the computed S_1 and T_2 adiabatic energies lies within the confidence range of the SCS-CC2 method. Therefore we cannot exclude the possibility that the $^3n_O\pi^*$ state is in fact degenerate with or lower than the $^1\pi\pi^*$ state. For this reason we tested the influence of this energy separation on the ISC rate constant. When the T_2 potential energy surface is lowered by values between 800 and 1000 cm^{-1}, the rate constants for the vibrationally cold $S_1, v = 0 \rightsquigarrow T_2$ transition are obtained in the range between 10^{10} and $10^{11}\ \mathrm{s}^{-1}$. It should be mentioned, however, that the computed rate constants vary substantially with the energy shift due to the low density of vibrational states in the T_2 state in this energy regime.

III. EXPERIMENTAL METHODS AND RESULTS

The experimental setup has been described previously.[15,66] Briefly, Ne (Linde, ≥99.995%) at $p = 1.8$ bar backing pressure is passed through a pulsed nozzle (0.4 mm diameter) containing cytosine (Sigma, >99% purity) heated to 235 °C. The jet-cooled keto-amino cytosine is excited with 200 μJ/pulse UV pulses from a frequency-doubled Radiant Dyes NarrowScan dye laser and ionized by tunable UV pulses in the 215-226 nm range (~150-200 μJ, ~10 cm^{-1} bandwidth) from an Ekspla NT342B ultraviolet optical parametric oscillator (UV-OPO). Delayed ionization measurements involved first exciting at the 0_0^0 band or one of the seven vibronic bands up to +437 cm^{-1} and then ionizing with a nanosecond time delay that was varied from 0-1000 ns, controlled by a DG535 digital delay unit. The S_1 population of **1** undergoes ISC to a triplet state that gives rise to an ion signal that decays with a lifetime of several 100 ns.[12–15,66] The resolution of the delayed ionization measurements is determined by the pulse widths of the two lasers (5-7 ns) and the relative trigger jitter, giving an instrumental response function of ~9 ns. Although internal conversion and intersystem crossing occurs about 10-15 times faster, the ratio of these rate constants k_{IC}/k_{ISC} can be accurately fitted from the relative amplitudes of the $^1\pi\pi^*$ and triplet state contributions to the total ion signal, see below.

Figure 4 shows the R2PI spectrum of jet-cooled Cyt in the frequency range 31 200–32 400 cm^{-1} when ionizing at 226 nm. The spectrum shows a sharp 0_0^0 band at 31 835 cm^{-1} (3.947 eV) and five medium to strong vibronic bands up to +205 cm^{-1}, with ten weaker bands between +277 and +530 cm^{-1}. The spectrum is similar to that reported by de Vries and co-workers,[12–14] who also reported that a part of the keto-amino cytosine population excited at the 0_0^0 band relaxes to a long-lived state that decays with a lifetime of

TABLE II. SCS-CC2/aug-cc-pVTZ calculated rotational constants (MHz) of the S_0 state, rotational constant changes relative to the S_1 ($\pi\pi^*$) state, the respective $S_0 \rightarrow S_1$ transition dipole moment orientations in the molecule-fixed inertial axis frame, and comparison to the experimental data, for cytosine, 5-methylcytosine, and 5-fluorocytosine. The estimated experimental errors are given in parentheses.

Molecule	A''	B''	C''	$A'-A''$	$B'-B''$	$C-C''$	$\lvert\mu_a\rvert^2:\lvert\mu_b\rvert^2:\lvert\mu_c\rvert^2$
Cytosine	3857	2012	1323	−80	−26	−9	7:91:2
Expt.[a]				−96(80)			5(6):95(9):0(5)
5-Methylcytosine	3137	1412	980	−103	1	−3	13:75:12
Expt.[b]				−118(80)			26(10):74(9):0(3)
5-Fluorocytosine	3188	1407	976	−127	6	0	15:81:4
Expt.[c]				−110(70)	(6)	(−1)	4(6):96(9):0(5)

[a]Reference 16.
[b]Reference 41.
[c]Reference 72.

several 100 ns, long enough to be measured by temporally delaying the ionization laser pulse. When photoionizing at 193 nm, Nir *et al.* measured a lifetime of τ_T = 290 ns, based on which they tentatively assigned it to a triplet state.[13] In our experiments we tune the 5 ns pulses from the UV OPO from the ionization threshold of the S_1 state, which lies at 38 600 cm^{-1} (4.79 eV) beyond the ionization threshold of the long-lived state at 44 200 cm^{-1} (5.48 eV). From this energy difference, the energy of the long-lived state has been determined as 3.26-3.37 eV above the S_0 state, in good agreement with our theoretical SCS-CC2 values of the T_1 ($^3\pi\pi^*$) energy and previous TDDFT results for keto-amino cytosine.[15] Figure 5 shows the analogous (R2PI) spectrum of jet-cooled 5-methylcytosine.

The photoionization efficiency (PIE) curves following excitation at the 0_0^0 band for prompt ionization (0 ns delay) and with delayed ionization (100 ns delay) have been given and discussed,[15] and we only briefly review the salient points: With prompt ionization, an onset in the PIE curve is observed at 38 600 cm^{-1}. The sum of the $S_0 \rightarrow S_1\, 0_0^0$ frequency (31 386 cm^{-1}) and the PIE threshold frequency (39 510 ± 78 cm^{-1}) corresponds to an adiabatic ionization potential of 8.73 ± 0.02 eV. In contrast, the onset of the PIE curve for delayed ionization is offset by about 4600 cm^{-1} to higher energy with a slow initial rise above the background. The rise of the delayed ionization PIE curve corresponds to ionization out of vibrationally hot levels that are produced by relaxation to the long-lived state.[15]

Figure 6(a) shows a time-delay scan of the ionization pulse relative to the excitation pulse on the 0_0^0 band. The rise and fall around 0 ns (prompt ionization) reflect the ion signal contribution from the optically excited S_1 state $v = 0$ level, the later near-constant part of the signal reflects the contribution from triplet state(s) that are populated by ISC out of the $v = 0$ level.[13,15] For a quantitative evaluation of the k_{ISC} rate constant, we assume that the only decay channels accessible

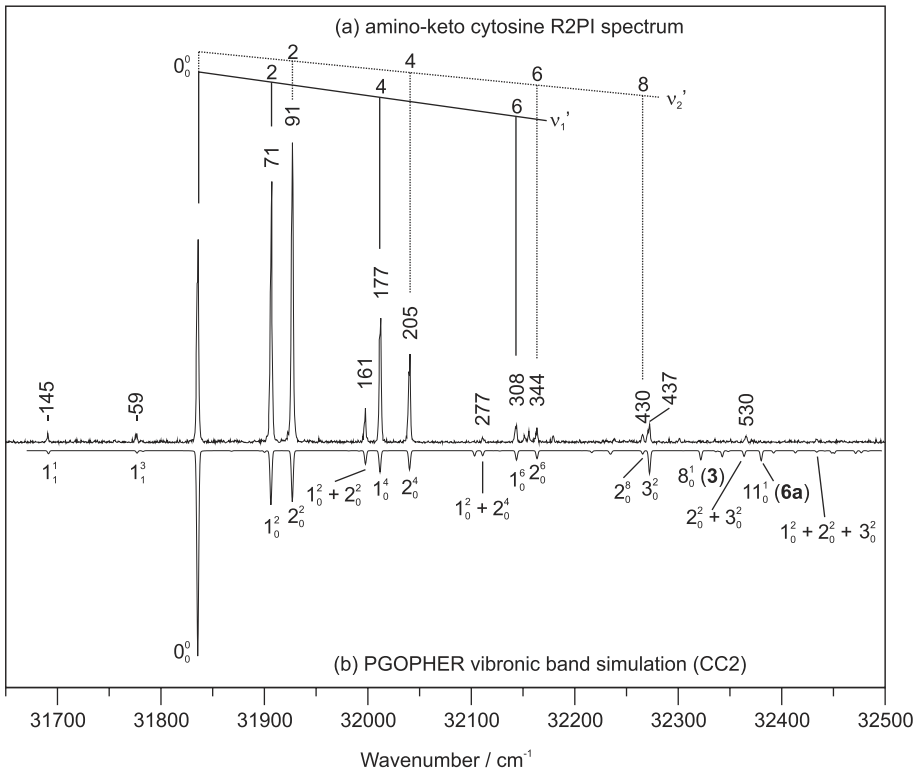

FIG. 4. Two-color resonant two-photon ionization spectrum of jet-cooled cytosine with vibronic band assignments, based on CC2 calculations (adapted from Figure 3 of Ref. 16). The wavenumber scale is relative to the 0_0^0 band at 31 835 cm^{-1}. Reproduced by permission of IOP Publishing Ltd.

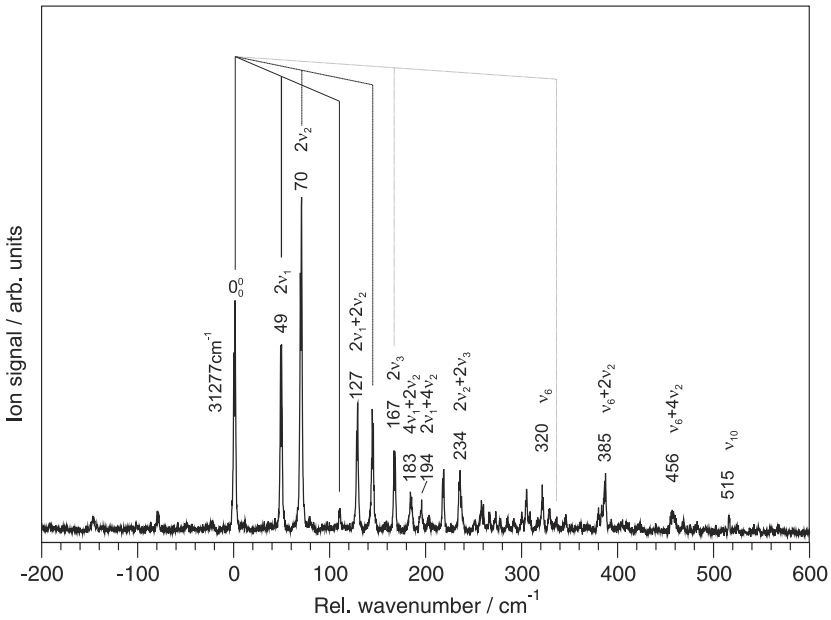

FIG. 5. Two-color resonant two-photon ionization spectrum of jet-cooled 5-methylcytosine with vibronic band assignments, based on CC2 calculations (adapted from Figure 4 of Ref. 41). The wavenumber scale is relative to the 0_0^0 band at 31 277 cm^{-1}. Reproduced by permission of IOP Publishing Ltd.

to $^1\pi\pi^*$ Cyt at low excess energy are fluorescence, $^1\pi\pi^* \rightsquigarrow S_0$ internal conversion and ISC with rate constants k_{rad}, k_{IC}, and k_{ISC}, respectively. The observed S_1 state decay rate constants, which have been determined in Ref. 16 via the vibronic-level specific lifetimes $\tau_{v,S_1} = (k_{v,S_1})^{-1}$, are then given by the sum of the decay rates $k_{v,S_1} = k_{rad} + k_{IC} + k_{ISC}$. Since the radiative rate constant k_{rad} for keto-amino cytosine is $k_{rad} \sim 3 \cdot 10^7$ s^{-1} we will neglect it relative to $k_{IC} + k_{ISC}$.

Based on El-Sayed's rules,[67] ISC from the $^1\pi\pi^*$ state is expected to occur most efficiently to $^3n\pi^*$ triplet states, that is to the T_2 state and *not* directly to the T_1 state, which is $^3\pi\pi^*$. For the closely related 5-methyl-2-hydroxypyrimidine, Pohler *et al.* have recently shown that the rapid ISC from the S_1 state[66] indeed proceeds by a related $S_1 \rightsquigarrow T_2$ El-Sayed-allowed ISC mechanism.[68] In the latter case, the T_2 state rapidly relaxes to T_1, so that our determination of k_{ISC} via ionization of the T_1 state includes the $T_2 \rightsquigarrow T_1$ internal conversion rate. Finally, the $T_1 \rightarrow S_0$ reverse ISC rate is denoted $k_T = (\tau_T)^{-1}$. The time dependence of the sum of the singlet and triplet-state populations can then be modeled as:[69]

$$I(t) = \frac{[S_1^0]}{k_{obs} - k_T}[(k_{v,S_1} - k_{ISC} - k_T)e^{-t/\tau_S} + k_{ISC}e^{-t/\tau_T}] = Ae^{-t/\tau_S} + Be^{-t/\tau_T}. \quad (1)$$

In order to account for the pulse width of the two lasers as well as the excited state lifetime (which is shorter than the laser pulses) the singlet and triplet parts of the equation were multiplied with the convolution of the instrument response function $E(t')$.[69]

$$I(t) = Ae^{-t/\tau_S}\int_0^t E(t')e^{(t'/\tau_S)}dt' + Be^{-t/\tau_T}\int_0^t E(t')e^{(t'/\tau_T)}dt'. \quad (2)$$

The instrument response function (IRF) is given by the convolution of the laser excitation and ionization pulse widths, which are approximate Gaussians of ~6 ns full width at half-maximum (FWHM), resulting in a Gaussian with ~8.5 ns FWHM. This has in turn to be convoluted with a third Gaussian that represents the time distribution of the trigger jitter of the two pulses. The width of the IRF was determined at an ionization wavelength >226 nm, at which only singlet (and no triplet) ionization occurs, and was found to be ~9 ns FWHM.

The quantum yield for ISC can then be expressed as[69]

$$Q_{ISC} = \frac{k_{ISC}}{k_{obs}} = \frac{B}{A+B}\left(1 - \frac{k_T}{k_{obs}}\right) \approx \frac{B}{A+B}. \quad (3)$$

The intersystem crossing quantum yields Q_{ISC} were determined for the $v = 0$ level and seven following S_1 state vibronic levels up to $E_{exc} = +437$ cm^{-1}. The time-delay scans for these eight vibrations are shown in Figure 6. On this time scale up to 50 ns after the pump pulse the $T_1 \rightarrow S_0$ ISC rate is almost unmeasurable, the experimental lifetime being $\tau = 290$ ns.[13] The level-specific ISC quantum yields were fitted to Equations (1) and (2) with a home-written IDL program using a Levenberg- Marquardt nonlinear least-squares fit. The S_1 (green) and T_1 (blue) population contributions to the fit are indicated in Figure 6, where the total fit is plotted in red. The analogous time-delay scans for five lowest vibronic levels of 5-methylcytosine,[41] with ionization at 215 nm are shown in Figure 7.

In Equations (1) and (2) the ionization cross sections of the S_1 and T_1 states are implicitly assumed to be identical, $\sigma_{ion}(S_1) = \sigma_{ion}(T_1)$. If the energy of the ionization photon is increased far beyond the adiabatic IP, these cross sections must become similar, $\sigma_{ion}(S_1)/\sigma_{ion}(T_1) \equiv \eta_{rel} \sim 1$, since the electron is ionized out of the same π^*-orbital. At the low ionization energies employed in our experiments this assumption is not justified, since (1) the geometries of the S_1 and T_1 states differ, hence the Franck-Condon factors in ionization to the ion ground states D_0 are different. (2) Ionization from the S_1 state occurs from the optically excited vibronic levels, while ISC produces the triplet cytosine with ~4600 cm^{-1} internal energy.[15] (3) The 215 nm ionization pulses ionize this "hot" T_1 state to about 3000 cm^{-1} above the triplet photoionization

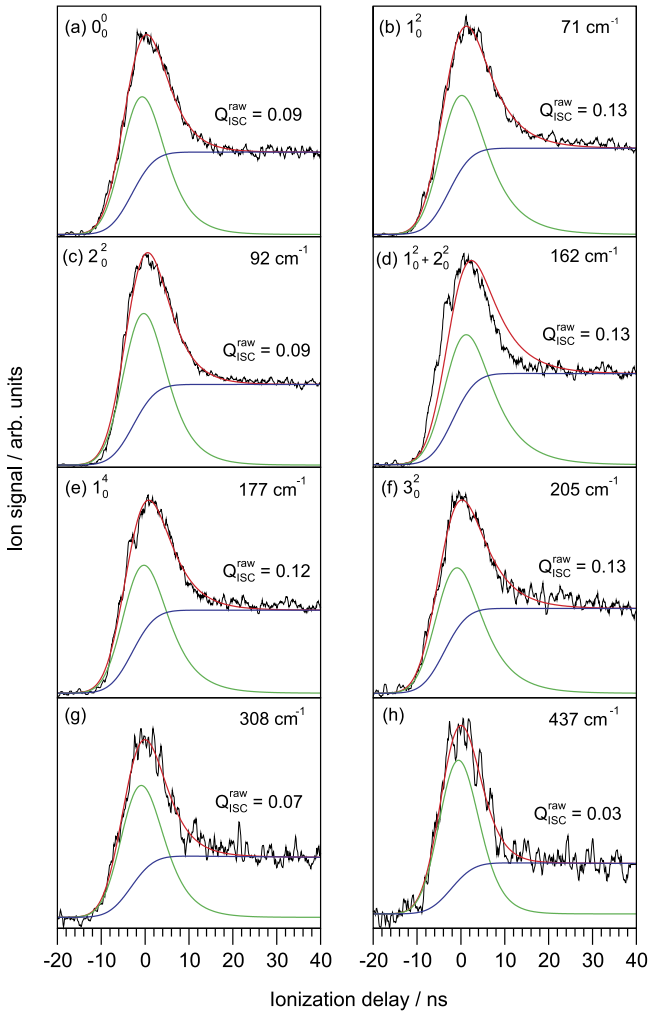

FIG. 6. Nanosecond UV pump/delayed ionization curves of keto-amino cytosine (a) with excitation at the $S_0 \rightarrow S_1\, 0_0^0$ band, ((b)–(h)) with excitation at the seven most intense vibronic bands shown in Figure 4. Ionization at 215 nm. Kinetic fits to the S_1 and triplet state ion signal contributions are shown in black and blue, respectively, the fit to the total ion signal is in red.

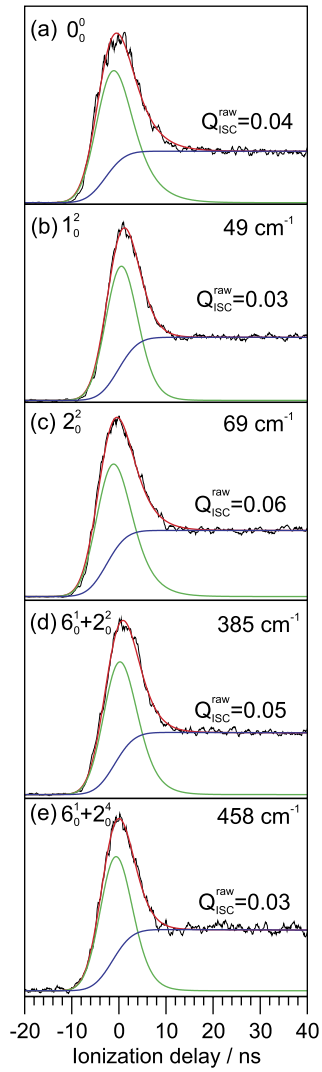

FIG. 7. Nanosecond UV pump/delayed ionization curves of keto-amino 5-methylcytosine excited via the 0_0^0 and seven vibronically excited bands shown in Figure 5, with ionization at 215 nm. Contributions from the S_1 and triplet state populations are indicated in black and blue, respectively. The fit to the total ion signal is given in red.

threshold,[15] while the S_1 state is ionized to ~7900 cm^{-1} above the adiabatic ionization threshold. Therefore, the intersystem crossing quantum yields given in Figure 6 for cytosine and Figure 7 for 5-methylcytosine are uncorrected values Q_{ISC}^{raw}.

To correct the Q_{ISC}^{raw} values we calculated the dependence of the σ_{ion} (S_1) and σ_{ion} (T_1) cross sections of cytosine on the ionization energy by evaluating the Franck-Condon factors (FCFs) from the S_1 and T_1 states to the ion ground state D_0. Figure 8(a) shows the $S_1(v = 0) \rightarrow D_0$ FCFs in black and the $T_1(v = 0) \rightarrow D_0$ FCFs in red. The S_1, T_1, and D_0 geometries were optimized and their respective harmonic vibrational frequencies and eigenvectors calculated at the SCS-CC2/aug-cc-pVDZ level. The ionization FCFs were calculated using PGOPHER 7.0.[70] Vibronic transitions from the S_1 and T_1 state $v = 0$ levels were calculated to all vibrational levels of the ion within the space of the four vibrations with the *largest* relative displacements (Huang-Rhys factors) between S_1 and D_0, or T_1 and D_0. The FCFs are convoluted with an ionization threshold function that is assumed to be a $0 \rightarrow 1$ step function at the adiabatic ionization threshold[15,71] in this near-threshold region. Figure 8(b) shows the respective calculated $S_1(v = 0) \rightarrow D_0$ and $T_1(v = 0) \rightarrow D_0$ PIE curves. The calculated S_1 PIE curve is very similar to the experimental PIE curve, which is shown in Figure 8(c). On the other hand, the calculated T_1 PIE curve in Figure 8(b) is offset by about +1000 cm^{-1} relative to the experimental curve in Figure 8(c). According to point (2), the $S_1 \rightsquigarrow T_1$ ISC produces vibrationally hot T_1 molecules with ~4600 cm^{-1} internal energy. The reason for the shift of the experimental T_1 PIE curve is the quasi-thermal PIE tail to low energy that is not included in the simulation.

Based on Figure 8(b) we estimate the relative singlet and triplet ionization cross sections as $\sigma_{ion}(S_1)/\sigma_{ion}(T_1)$ ~3 at the ionization wavelength of 215 nm. This estimate may be on the low side, because the geometry difference between T_1 and D_0 is larger than that between S_1 and D_0, as the width of the FCF distribution in Figure 8(a) shows. Since our PIE curve simulation can only account for the geometry change along the four normal modes with the largest Huang-Rhys factors, we expect the relative importance of the neglected vibrations

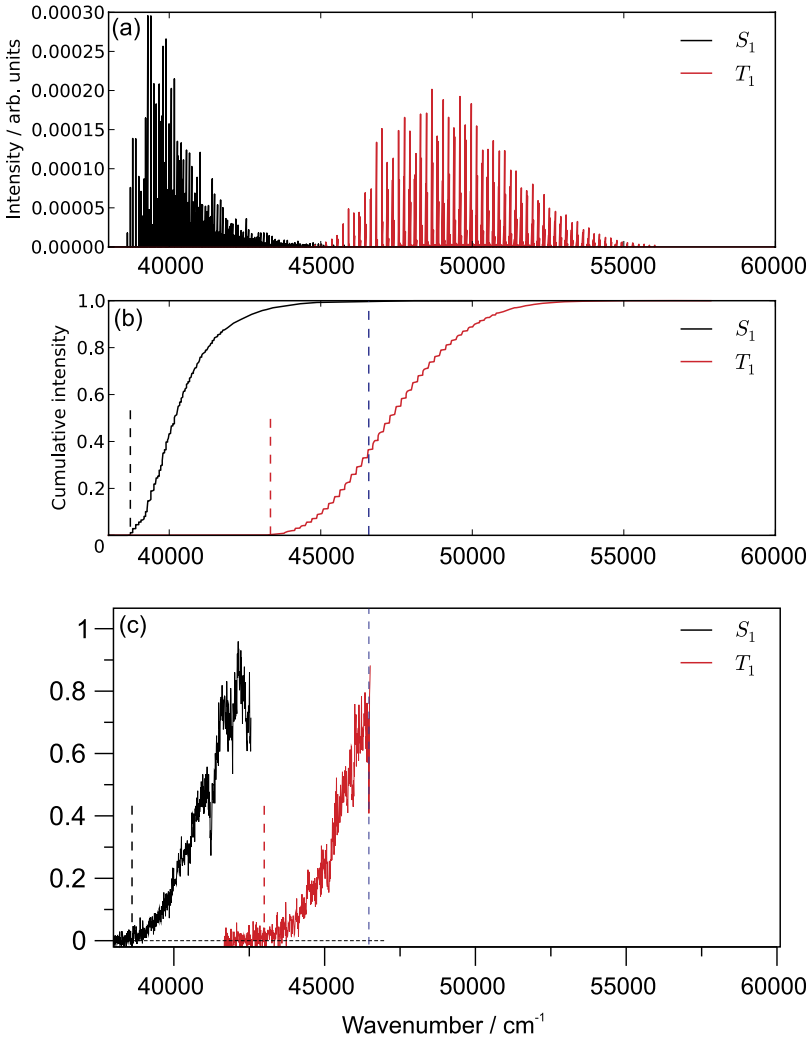

FIG. 8. (a) Calculated ionization Franck-Condon factors (FCFs) from the S_1 and T_1 excited-state vibrationless $v = 0$ levels to the ion ground state (D_0): $S_1(v = 0) \rightarrow D_0$ FCFs in black, $T_1(v = 0) \rightarrow D_0$ FCFs in red, plotted vs. the energy of the ionization photon in cm^{-1}. (b) Calculated photoionization efficiency (PIE) curves of the S_1 and T_1 states using the FCFs from panel (a). Vertical black red and blue dashed lines indicate the adiabatic ionization threshold (vibrationless $S_1 \rightarrow D_0$ and $T_1 \rightarrow D_0$ transitions, respectively. The dashed blue line indicates the experimental ionization energy (215 nm). (c) Experimental PIE curves of amino-keto cytosine S_1 state (undelayed or "prompt" ion signal) and T_1 state, data taken from Ref. 15. For further details see the text.

(with smaller Huang-Rhys factors) to be larger for $T_1 \rightarrow D_0$ ionization.

We note that in Ref. 13, ionization of the cytosine excited states was performed with an ArF excimer laser at a wavelength of 193 nm. At this higher ionization energy (51 800 cm^{-1}), Figure 8(b) predicts that the triplet photoionization cross section increases further, relative to the singlet photoionization cross section. Since $\sigma_{ion}(S_1)/\sigma_{ion}(T_1)$ now approaches ~1, the S_1 and T_1 states are ionized with almost the same probability. This should remove the "shoulders" in the time-delay profiles, as compared to Figs. 6 and 7. This prediction of our Franck-Condon model is in perfect agreement with the experimental 193 nm time-delay profile in Fig. 3 of Ref. 13, which does not exhibit a shoulder.

Based on Figure 8, we corrected the Q_{ISC}^{raw} values in Figures 6 and 7; the corrected ISC yields Q_{ISC}^{corr} are given in Tables III and IV. Combining these Q_{ISC}^{corr} values with the experimental S_1 state lifetimes τ_{obs} determined for the same vibronic levels of cytosine,[16] which are given in column 2 of Table III then allows to determine the internal conversion and intersystem crossing rate constants k_{IC} and k_{ISC} as a function of vibrational excess energy E_{exc}. As Table III shows, the experimental ISC rate constants are in the range

TABLE III. Experimental lifetimes, intersystem crossing quantum yields Q_{ISC} and k_{ISC} parameters of keto-amino cytosine.

Vibronic transition	τ_{obs} / 5 ps	Q_{ISC}^{raw}	$Q_{ISC}^{corr a}$	k_{ISC} /10^9 s^{-1}	k_{IC} /10^{10} s^{-1}
0_0^0	44 (5)	0.09	0.03	0.68	2.2
1_0^2 (71 cm^{-1})	33 (5)	0.13	0.05	1.5	2.9
2_0^2 (92 cm^{-1})	33 (5)	0.09	0.03	0.91	2.9
$1_0^2+2_0^2$ (162 cm^{-1})	38 (4)	0.13	0.05	1.3	2.5
1_0^4 (177 cm^{-1})	33 (3)	0.12	0.04	1.2	2.9
3_0^2 (205 cm^{-1})	44 (4)	0.13	0.05	1.1	2.2
308 cm^{-1}	>25	0.07	0.03	1.2	<3.9
437 cm^{-1}	>25	0.03	0.01	0.40	<3.9

[a]Assuming relative ionization cross section $\sigma_{ion}(S_1)/\sigma_{ion}(T_1) = 3$.

TABLE IV. Experimental lifetimes, intersystem crossing quantum yields Q_{ISC} and k_{ISC} parameters of keto-amino 5-methylcytosine.

Vibronic transition	τ_{obs}/ps	Q_{ISC}^{raw}	$Q_{ISC}^{corr a}$	k_{ISC} /10^9 s^{-1}	k_{IC} /10^{10} s^{-1}
0_0^0	60 (5)	0.04	0.02	0.33	1.6
1_0^2 (49 cm^{-1})	60 (5)	0.03	0.01	0.17	1.6
1_0^2 (69 cm^{-1})	60 (5)	0.06	0.02	0.33	1.6
$6_0^1+2_0^2$ (385 cm^{-1})	...	0.05	0.02	...	...
$6_0^1+2_0^4$ (458 cm^{-1})	...	0.03	0.01	...	...

[a]Assuming relative ionization cross section $\sigma_{ion}(S_1)/\sigma_{ion}(T_1) = 3$.

$0.4–1.6 \cdot 10^9$ s^{-1}, while the experimental IC rate constants are much higher, being in the range $2.2–3.9 \cdot 10^{10}$ s^{-1} or 30–100 times the ISC rate constants. Upon correcting the raw ISC yields shown in Figure 7 for 5-methylcytosine with the same relative ionization efficiency factor $\sigma_{ion}(S_1)/\sigma_{ion}(T_1) \sim 3$, we obtain the corrected Q_{ISC}^{corr} values and the ISC and IC rate constants given in Table IV.

IV. DISCUSSION

If the energetic ordering of the S_1 and T_2 states of keto-amino Cyt obtained from the SCS-CC2 calculations is correct, then only the $S_1 \rightsquigarrow T_1$ ISC channel is open from the vibrationally cold $v = 0$ S_1 state. Our calculated ISC rate constant for this process ($3 \cdot 10^9$ s^{-1}) is four times the experimental value $k_{ISC} = 0.7 \cdot 10^9$ s^{-1}. Given the uncertainties involved in both theory and experiment, this agreement is remarkably good. Results obtained for cytosine derivatives support this mechanism, which was also advocated by Merchán and co-workers.[64] The calculated and experimental adiabatic excitation energies and vibrationless (0_0^0) transition energies of the S_1, T_1, and T_2 states of cytosine, 5-methylcytosine,[41] and 5-fluorocytosine[72] are collected in Table I. It is seen that the adiabatic energy differences between the S_1 and T_1 states of the three compounds are similar; in contrast, the energy gap between the S_1 and T_2 states of cytosine and 5-methylcytosine differs substantially. While it is debatable whether the $v = 0$ level of the T_2 state is located energetically above S_1 ($v' = 0$) in cytosine, this is clearly not the case in the 5-methyl derivative where these levels are 0.36 eV apart. Hence, it can safely be assumed that the $S_1 \rightsquigarrow T_2$ ISC can only occur as a thermally activated process in 5MCyt. Nevertheless, the experimental $0_0^0(^1\pi\pi^*)$ lifetimes of jet-cooled 5-methylcytosine (60 ps) and 5-fluorocytosine (75 ps) are of the same order of magnitude as that of cytosine (45 ps).[15,16,41,72] We therefore conclude that the dominant ISC mechanism of the vibrationally cold S_1 state of cytosine in the gas phase is the direct $S_1, v = 0 \rightsquigarrow T_1$ intersystem crossing.

As soon as the T_2 ISC channel becomes energetically accessible, the calculated ISC rates increase by one to two orders of magnitude, depending on the exact energy separation between the initial and final states. Despite the considerable spread in our theoretical results, we are confident that the decay rates are substantially smaller than the values predicted by Richter *et al.*[32] and Mai *et al.*[33] These authors claimed the $S_1 \rightsquigarrow T_2$ transition to occur on an ultrafast (subpicosecond) time scale. However, their excited-state surface hopping dynamics treatment is based on state-averaged CASSCF energies and wave functions. At that level of theory, the global minimum of the S_1 potential energy surface corresponds to a $^1n_O\pi^*$ electronic structure[30,64] which was proven to be not correct by recent experimental investigations.[15,72] According to our present calculations, the $S_1 \rightsquigarrow T_2$ ISC cannot be responsible for the experimentally observed ultrafast decay of the S_1 state, which begins about 530 cm^{-1} above the origin.[16] For the vibrational levels located above this threshold, ultrafast internal conversion to the S_0 state via a conical intersection is believed to be the dominating process.

Overall, we note that the intersystem crossing quantum yields and rates are similar to that measured for thymine isomer 5-methyl-2-hydroxypyrimidine, for which ISC is the dominant nonradiative process out of the S_1 state, with $k_{ISC} \sim 1/\tau_{fl} \sim 2 \cdot 10^{10}$ s^{-1}.[66]

V. CONCLUSIONS

We show experimentally and by *ab initio* calculations that the keto-amino tautomers of supersonically cooled cytosine and 5-methylcytosine undergo moderately efficient intersystem crossing from their photoexcited $S_1(^1\pi\pi^*)$ states[12,15] to the triplet $T_1(^3\pi\pi^*)$ state. We experimentally quantify the ISC quantum yields (Q_{ISC}) and rates (k_{ISC}) as a function of the S_1 state vibrational excess energy E_{exc} by separately detecting the S_1 and T_1 states using prompt and delayed laser photoionization. The relative S_1 and T_1 ionization cross sections are calculated from the SCS-CC2 calculated S_1, T_1 and ion D_0 state geometries and frequencies, followed by calculation of the photoionization Franck-Condon factors. The ionization-corrected ISC quantum yields are in the range $Q_{ISC}^{corr} = 0.01–0.05$ for the lowest eight vibronic levels of cytosine and $Q_{ISC}^{corr} = 0.01–0.02$ for the lowest three levels of 5-methylcytosine.

Combining these Q_{ISC}^{corr} values with the experimental S_1 state lifetimes that were previously determined for the same vibronic levels of cytosine[16] and of 5-methylcytosine[41] allows to determine both the ISC and IC rates k_{ISC} and k_{IC}. The ISC rates for S_1 state cytosine up to $E_{exc} \sim 550$ cm^{-1} are $k_{ISC} \sim 0.4–1.5 \cdot 10^9$ s^{-1}. For 5-methylcytosine the ISC rates of the lowest three levels are $k_{ISC} \sim 0.3 \cdot 10^9$ s^{-1}.

Theoretical ISC rates are calculated using the spin-component-scaled SCS-CC2 method with the aug-cc-pVTZ basis set. These predict rapid ISC from the $S_1, v = 0$ state with $k_{ISC} = 3 \cdot 10^9$ s^{-1} to the $T_1(^3\pi\pi^*)$ triplet state. The surprisingly high rate of this El Sayed-forbidden transition is caused by a substantial admixture of $^1n_O\pi^*$ character into the $S_1(^1\pi\pi^*)$ wave function at its non-planar minimum geometry. Results on 5-methylcytosine and 5-fluorocytosine support this mechanism. The vibrational ground state of the $T_2(^3n_O\pi^*)$ triplet state of cytosine is located ~650 cm^{-1} above the $S_1, v = 0$ level. As soon as the T_2 channel becomes energetically available, ISC rates increase by one to two orders of magnitude, depending on the excess energy.

For the low-lying vibronic levels of cytosine and 5-methylcytosine investigated, the level-specific $S_1 \rightsquigarrow S_0$ IC rate constants are 20–50 times faster than the corresponding ISC rate constants, so internal conversion is clearly the dominant nonradiative process near the minimum of the S_1 state. Above $E_{exc} \sim 600$ cm^{-1} no further vibronic bands are observed, implying that the IC rate increases by a factor of ≥50 within about 150 cm^{-1}.[16] This agrees[16] with the experimental observation of short lifetimes $\tau \leq 2$ ps measured by femtosecond two-step laser photoionization techniques at higher E_{exc}.[39,40] Above this energy, we detect no triplet state ion signals (ISC quantum yield $Q_{ISC} \leq 0.01$), which implies that $S_1 \rightarrow S_0$ internal conversion effectively shuts off both the $S_1 \rightsquigarrow T_1$ and $S_1 \rightsquigarrow T_2$ ISC decay channels. The sudden

increases in k_{IC} imply that the barrier towards the lowest conical intersection (C5-twist CI)[1,17–30] is surmounted around E_{exc} = 550 cm^{-1}.

Our calculated and experimental ISC rate constants are 1000–10 000 times smaller than those of previous calculations that predicted ultrafast ISC of cytosine with $k_{ISC} = 10^{13}$–10^{14} s^{-1}.[32,33] Our calculations address the low-lying vibronic levels of S_1 cytosine, while the previous predictions were computed using broad-band excitation in the range from 4–7 eV (177–310 nm), corresponding to excitation at very high energy.[32,33] While broadband excitation extending far into the deep UV may be interesting from a theoretical point of view, the solar UV radiation that leads to modern-day DNA photochemistry and photodamage is cut off by the earth's ozone layer around 295–300 nm. In fact, the region of low E_{exc} probed in our experiments and calculations corresponds to the long-wavelength "red edge" absorption of cytosine in solution.[5,73] This is the primary region of photobiological and -medical interest with respect to UV lesions and skin cancer,[73] and not the vertical excitation to the absorption band maximum at ~260 nm.[32,33]

In summary, we show that upon exciting gas-phase S_1 state keto-amino cytosine from the 0_0^0 band up to $E_{exc} \sim 440$ cm^{-1}, neither $S_1 \rightsquigarrow S_0$ internal conversion[16] nor $S_1 \rightsquigarrow T_1$ intersystem crossing are ultrafast. Internal conversion is the most efficient nonradiative channel, being 30–40 times faster than ISC. The ISC quantum yield of cytosine and cytidine in aqueous solution is $Q_{ISC} \sim 0.02$,[10,11] very close to that determined here for cold gas-phase cytosine. However, the IC rate of cytosine and cytidine in aqueous solution measured with excitation at 263-270 nm (that is, at photon energies ~5600 cm^{-1} higher than in this work) is $k_{IC} \sim 6$–$13 \cdot 10^{11}$ s^{-1} (Refs. 6–8) or about 30 times faster than in the gas-phase at low excess energy E_{exc}.[16] This implies that at this much higher excess energy, the k_{ISC} in room temperature aqueous solution also increases by ~30×. It will be interesting to investigate the nonradiative properties of cytosine close to its electronic origin also in aqueous solution, and also to probe the effects of H-bonding interactions with proximal water molecules[74] on the gas-phase photophysics of cytosine.

ACKNOWLEDGMENTS

Financial support by the Schweiz. Nationalfonds (Project Nos. 200020-121993 and 200020-152816) is gratefully acknowledged.

[1]M. Merchan and L. Serrano-Andrés, J. Am. Chem. Soc. **125**, 8108 (2003).
[2]B. Brauer, R. B. Gerber, M. Kabelač, P. Hobza, J. M. Bakker, A. G. A. Riziq, and M. S. de Vries, J. Phys. Chem. A **109**, 6974 (2005).
[3]M. K. Shukla and J. Leszczynski, *Radiation Induced Molecular Phenomena in Nucleic Acids* (Springer, Netherlands, 2008), pp. 1–14.
[4]L. Serrano-Andrés and M. Merchan, J. Photochem. Photobiol., C **10**, 21 (2009).
[5]C. T. Middleton, K. de La Harpe, C. Su, Y. K. Law, C. E. Crespo-Hernandez, and B. Kohler, Annu. Rev. Phys. Chem. **60**, 217 (2009).
[6]J. M. Pecourt, J. Peon, and B. Kohler, J. Am. Chem. Soc. **123**, 10370 (2001).
[7]J. Peon and A. H. Zewail, Chem. Phys. Lett. **348**, 255 (2001).
[8]R. J. Malone, A. M. Miller, and B. Kohler, Photochem. Photobiol. **77**, 158 (2003).
[9]P. Vigny, C. R. Acad. Sci., Ser. D **272**, 2247 (1971).
[10]J. Cadet and P. Vigny, "The photochemistry of nucleic acids in bioorganic photochemistry," in *Bioorganic Photochemistry, Photochemistry and the Nucleic Acids*, edited by H. Morrison (Wiley, New York, 1990), pp. 1–272.
[11]C. Salet, R. Bensasson, and R. Becker, Photochem. Photobiol. **30**, 325 (1979).
[12]E. Nir, C. Janzen, P. Imhof, K. Kleinermanns, and M. S. de Vries, Phys. Chem. Chem. Phys. **4**, 732 (2002).
[13]E. Nir, M. Müller, L. I. Grace, and M. S. de Vries, Chem. Phys. Lett. **355**, 59 (2002).
[14]E. Nir, I. Hünig, K. Kleinermanns, and M. S. de Vries, Phys. Chem. Chem. Phys. **5**, 4780 (2003).
[15]S. Lobsiger and S. Leutwyler, J. Phys. Chem. Lett. **3**, 3576 (2012).
[16]S. Lobsiger, M. A. Trachsel, H. M. Frey, and S. Leutwyler, J. Phys. Chem. B **117**, 6106 (2013).
[17]N. Ismail, L. Blancafort, M. Olivucci, B. Kohler, and M. Robb, J. Am. Chem. Soc. **124**, 6818 (2002).
[18]L. Blancafort and M. A. Robb, J. Phys. Chem. A **108**, 10609 (2004).
[19]K. Tomic, J. Tatchen, and C. M. Marian, J. Phys. Chem. A **109**, 8410 (2005).
[20]M. Z. Zgierski, S. Patchkovskii, T. Fujiwara, and E. C. Lim, J. Phys. Chem. A **109**, 9384 (2005).
[21]M. Z. Zgierski, S. Patchkovskii, T. Fujiwara, and E. C. Lim, J. Chem. Phys. **123**, 081101 (2005).
[22]L. Blancafort, B. Cohen, P. M. Hare, B. Kohler, and M. A. Robb, J. Phys. Chem. A **109**, 4431 (2005).
[23]M. Merchán, R. González-Luque, T. Climent, L. Serrano-Andrés, E. Rodríguez, M. Reguero, and D. Peláez, J. Phys. Chem. B **110**, 26471 (2006).
[24]K. A. Kistler and S. Matsika, J. Phys. Chem. A **111**, 2650 (2007).
[25]K. A. Kistler and S. Matsika, J. Phys. Chem. A **111**, 8708 (2007).
[26]K. A. Kistler and S. Matsika, J. Chem. Phys. **128**, 215102 (2008).
[27]H. R. Hudock and T. J. Martínez, ChemPhysChem **9**, 2486 (2008).
[28]R. Gonzalez-Luque, T. Climent, L. Gonzalez-Ramirez, M. Merchán, and L. Serrano-Andrés, J. Chem. Theory Comput. **6**, 2103 (2010).
[29]T. Climent, I. Gonzalez-Ramirez, R. Gonzalez-Luque, M. Merchán, and L. Serrano-Andrés, J. Phys. Chem. Lett. **1**, 2072 (2010).
[30]M. Barbatti, A. J. A. Aquino, J. J. Szymczak, D. Nachtigallova, and H. Lischka, Phys. Chem. Chem. Phys. **13**, 6145 (2011).
[31]F. J. A. Ferrer, F. Santoro, and R. Improta, Comput. Theor. Chem. **1040–1041**, 186 (2014).
[32]M. Richter, P. Marquetand, J. González-Vázquez, I. Sola, and L. González, J. Phys. Chem. Lett. **3**, 3090 (2012).
[33]S. Mai, P. Marquetand, M. Richter, J. González-Vázquez, and L. González, ChemPhysChem **14**, 2920 (2013).
[34]M. Etinski, T. Fleig, and C. M. Marian, J. Phys. Chem. A **113**, 11809 (2009).
[35]M. Kunitski, Y. Nosenko, and B. Brutschy, ChemPhysChem **12**, 2024 (2011).
[36]H. Kang, K. T. Lee, B. Jung, Y. J. Ko, and S. K. Kim, J. Am. Chem. Soc. **124**, 12958 (2002).
[37]S. Ullrich, T. Schultz, M. Z. Zgierski, and A. Stolow, Phys. Chem. Chem. Phys. **6**, 2796 (2004).
[38]C. Canuel, M. Mons, F. Piuzzi, B. Tardivel, I. Dimicoli, and M. Elhanine, J. Chem. Phys. **122**, 074316 (2005).
[39]K. Kosma, C. Schröter, E. Samoylova, I. V. Hertel, and T. Schultz, J. Am. Chem. Soc. **131**, 16939 (2009).
[40]J. W. Ho, H.-C. Yen, W.-K. Chou, C.-N. Weng, L.-H. Cheng, H.-Q. Shi, S.-H. Lai, and P.-Y. Cheng, J. Phys. Chem. A **115**, 8406 (2011).
[41]M. A. Trachsel, S. Lobsiger, and S. Leutwyler, J. Phys. Chem. B **116**, 11081 (2012).
[42]A. Hellweg, S. A. Grün, and C. Hättig, Phys. Chem. Chem. Phys. **10**, 4119 (2008).
[43]N. O. C. Winter, N. K. Graf, S. Leutwyler, and C. Hättig, Phys. Chem. Chem. Phys. **15**, 6623 (2013).
[44]TURBOMOLE V6.5 2013, a development of University of Karlsruhe and Forschungszentrum Karlsruhe GmbH, 1989-2007, TURBOMOLE GmbH, 2007, available from http://www.turbomole.com.
[45]O. Vahtras, J. Almlöf, and M. W. Feyereisen, Chem. Phys. Lett. **213**, 514 (1993).
[46]C. Hättig and F. Weigend, J. Chem. Phys. **113**, 5154 (2000).
[47]C. Hättig, J. Chem. Phys. **118**, 7751 (2003).
[48]A. Köhn and C. Hättig, J. Chem. Phys. **119**, 5021 (2003).
[49]C. Hättig and A. Köhn, J. Chem. Phys. **117**, 6939 (2002).
[50]T. H. J. Dunning, J. Chem. Phys. **90**, 1007 (1989).

[51]R. A. Kendall, T. H. J. Dunning, and R. J. Harrison, J. Chem. Phys. **9**, 6796 (1992).
[52]F. Weigend, A. Köhn, and C. Hättig, J. Chem. Phys. **116**, 3175 (2002).
[53]J. Neugebauer, M. Reiher, C. Kind, and B. A. Hess, J. Comput. Chem. **23**, 895 (2002).
[54]C. Marian, "Spin-orbit coupling in molecules," in *Reviews in Computational Chemistry*, edited by K. Lipkowitz and D. Boyd (Wiley-VCH, Weinheim, 2001), Vol. 17, pp. 99–204.
[55]M. Kleinschmidt, J. Tatchen, and C. M. Marian, J. Comput. Chem. **23**, 824 (2002).
[56]B. Schimmelpfennig, *AMFI, An Atomic Mean-Field Spin-Orbit Integral Program* (Stockholms University, 1996).
[57]B. A. Hess, C. M. Marian, U. Wahlgren, and O. Gropen, Chem. Phys. Lett. **251**, 365 (1996).
[58]J. Tatchen, N. Gilka, and C. M. Marian, Phys. Chem. Chem. Phys. **9**, 5209 (2007).
[59]M. Etinski, J. Tatchen, and C. M. Marian, J. Chem. Phys. **134**, 154105 (2011).
[60]M. Etinski, V. Rai-Constapel, and C. M. Marian, J. Chem. Phys. **140**, 114104 (2014).
[61]M. Etinski, J. Tatchen, and C. M. Marian, Phys. Chem. Chem. Phys. **16**, 4740 (2014).
[62]See supplementary material at http://dx.doi.org/10.1063/1.4937375 for additional material on cytosine intersystem crossing.
[63]A. Nakayama, Y. Harabuchi, S. Yamazaki, and T. Taketsugu, Phys. Chem. Chem. Phys. **15**, 12322 (2013).
[64]M. Merchán, L. Serrano-Andrés, M. A. Robb, and L. Blancafort, J. Am. Chem. Soc. **127**, 1820 (2005).
[65]K. Kistler and S. Matsika, Phys. Chem. Chem. Phys. **12**, 5024 (2010).
[66]S. Lobsiger, H. M. Frey, S. Leutwyler, P. Morgan, and D. Pratt, J. Phys. Chem. A **115**, 13281 (2011).
[67]M. El-Sayed, Acc. Chem. Res. **1**, 8 (1968).
[68]L. Pohler, M. Kleinschmidt, M. Etinski, and C. M. Marian, Mol. Phys. **110**, 2429 (2012).
[69]R. G. Lipert, G. Bermudez, and S. Colson, J. Phys. Chem. **92**, 3801 (1988).
[70]C. M. Western, PGOPHER 7.0, a Program for Simulating Rotational, Vibrational and Electronic Structure, University of Bristol, 2013, pgopher.chm.bris.ac.uk.
[71]P. M. Guyon and J. Berkowitz, J. Chem. Phys. **54**, 1814 (1971).
[72]S. Lobsiger, M. A. Trachsel, T. Den, and S. Leutwyler, J. Phys. Chem. B **118**, 2973 (2014).
[73]W. J. Schreier, P. Gilch, and W. Zinth, Annu. Rev. Phys. Chem. **66**, 497 (2015).
[74]S. Lobsiger, R. K. Sinha, S. Blaser, H.-M. Frey, and S. Leutwyler, Nat. Chem. **6**, 989 (2014).
[75]O. Kostko, K. Bravaya, A. Krylov, and M. Ahmed, Phys. Chem. Chem. Phys. **12**, 2860 (2010).